# The Holocene

**Late-Holocene and Younger Dryas glaciers in the northern Cairngorm Mountains, Scotland**
Martin Kirkbride, Jez Everest, Doug Benn, Delia Gheorghiu and Alastair Dawson
*The Holocene* 2014 24: 141 originally published online 18 December 2013
DOI: 10.1177/0959683613516171

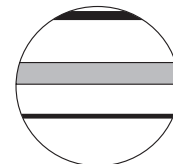The online version of this article can be found at:
http://hol.sagepub.com/content/24/2/141

>> Version of Record - Jan 20, 2014

OnlineFirst Version of Record - Dec 18, 2013

What is This?

# Late-Holocene and Younger Dryas glaciers in the northern Cairngorm Mountains, Scotland

**Martin Kirkbride,[1] Jez Everest,[2] Doug Benn,[3] Delia Gheorghiu[4] and Alastair Dawson[5]**

## Abstract

We present 17 cosmogenic [10]Be ages of glacial deposits in Coire an Lochain (Cairngorm Mountains), which demonstrate that glacial and nival deposits cover a longer timescale than previously recognised. Five ages provide the first evidence of a late-Holocene glacier in the British Isles. A previously unidentified moraine ridge was deposited after *c.* 2.8 kyr and defines a small slab-like glacier with an equilibrium line altitude (ELA) at *c.* 1047 m. The late-Holocene glacier was characterised by rapid firnification and a dominance of sliding, enabling the glacier to construct moraine ridges in a relatively short period. Isotopic inheritance means that the glacier may have existed as recently as the 'Little Ice Age' (LIA) of the 17th or 18th century AD, a view supported by glacier-climate modelling. Nine [10]Be ages confirm a Younger Dryas Stadial (YDS) age for a cirque-floor boulder till, and date the glacier maximum to *c.* 12.3 kyr when the ELA was at *c.* 963 m altitude. Both glaciers existed because of enhanced accumulation from wind-blown snow, but the difference in ELA of only *c.* 84 m belies the YDS–LIA temperature difference of *c.* 7°C and emphasises the glacioclimatic contrast between the two periods. Three [10]Be ages from till boulders originally deposited in the YDS yield ages <5.5 kyr and indicate snow-avalanche disturbance of older debris since the mid-Holocene, as climate deteriorated towards marginal glaciation.

## Keywords

beryllium 10, Cairngorm Mountains, cosmogenic dating, glacier reconstruction, 'Little Ice Age', Younger Dryas

Received 4 September 2013; revised manuscript accepted 15 November 2013

## Introduction

Scotland's last glaciers are generally accepted to have vanished at the close of the Younger Dryas Stadial (YDS), around 11.5 kyr (Golledge et al., 2008). Geomorphological evidence of Holocene glaciers has proved elusive, though a favourable climate for cirque glaciation in the 'Little Ice Age' (LIA, *c.* AD 1300–1850, Matthews and Briffa, 2005) is implied by historical accounts of year-round snow cover and lake ice in the 17th and 18th centuries, and by the small temperature depression calculated to be sufficient to allow net annual snow accumulation in high-altitude cirques (Harrison et al., forthcoming; Kington, 2010; Lamb, 1995; Manley, 1949; Sugden, 1977). Attention has focused on attempts to show that moraines ascribed to the YDS (locally termed the Loch Lomond Stadial or LLS) were actually late Holocene in age (Sugden, 1977), but ^{14}C dating of cirque lake sediments (Batterbee et al., 2001; Rapson, 1985) does not support a LIA age of cirque moraines in the northern Cairngorm Mountains. This paper reports cosmogenic [10]Be ages and glaciological reconstructions of cirque moraines in Coire an Lochain (Figure 1) to examine the evidence for both YDS and subsequent glacial advances.

## Geomorphological evidence

Several glacial and nival landforms are identified within the cirque (Figure 1). The cirque-floor boulder sheet was deposited as supraglacial melt-out till during retreat from the YDS maximum extent, and was ascribed a YDS age by Sissons (1979). The maximum glacier extent is clearly defined by its distal edge, although lack of a distinct terminal moraine ridge suggests that the maximal extent was short-lived. A lateral moraine can be traced up the eastern glacier margin, constraining reconstruction of the glacier ablation zone.

The cirque backwall comprises a debris slope leading up to the Great Slab, a stepped, plucked, low-angled (*c.* 25°–30°) granite slab which merges upslope with the vertical 100-m-high headwall (Figures 2 and 3a). The junction of slab and cliff is free of rockfall talus, in contrast to ledges elsewhere on the cirque walls. The rock scenery of the upper cirque is 'clean' and has been interpreted as the source of a pre-YDS rock slope failure by Ballantyne (2013). Bordering most of the east edge of the slab, and the lower west edge, are small but prominent steep-sided debris ridges, of which the eastern ridge extends for >100 m obliquely downslope (Figures 1 and 3b). The western ridge terminates abruptly upslope at a rock wall. The two ridges do not meet at the base of the Great

[1]University of Dundee, UK
[2]British Geological Survey, UK
[3]UNIS, Norway
[4]SUERC, UK
[5]University of Aberdeen, UK

**Corresponding author:**
Martin Kirkbride, University of Dundee, Nethergate, Dundee, DD1 4HN, UK.
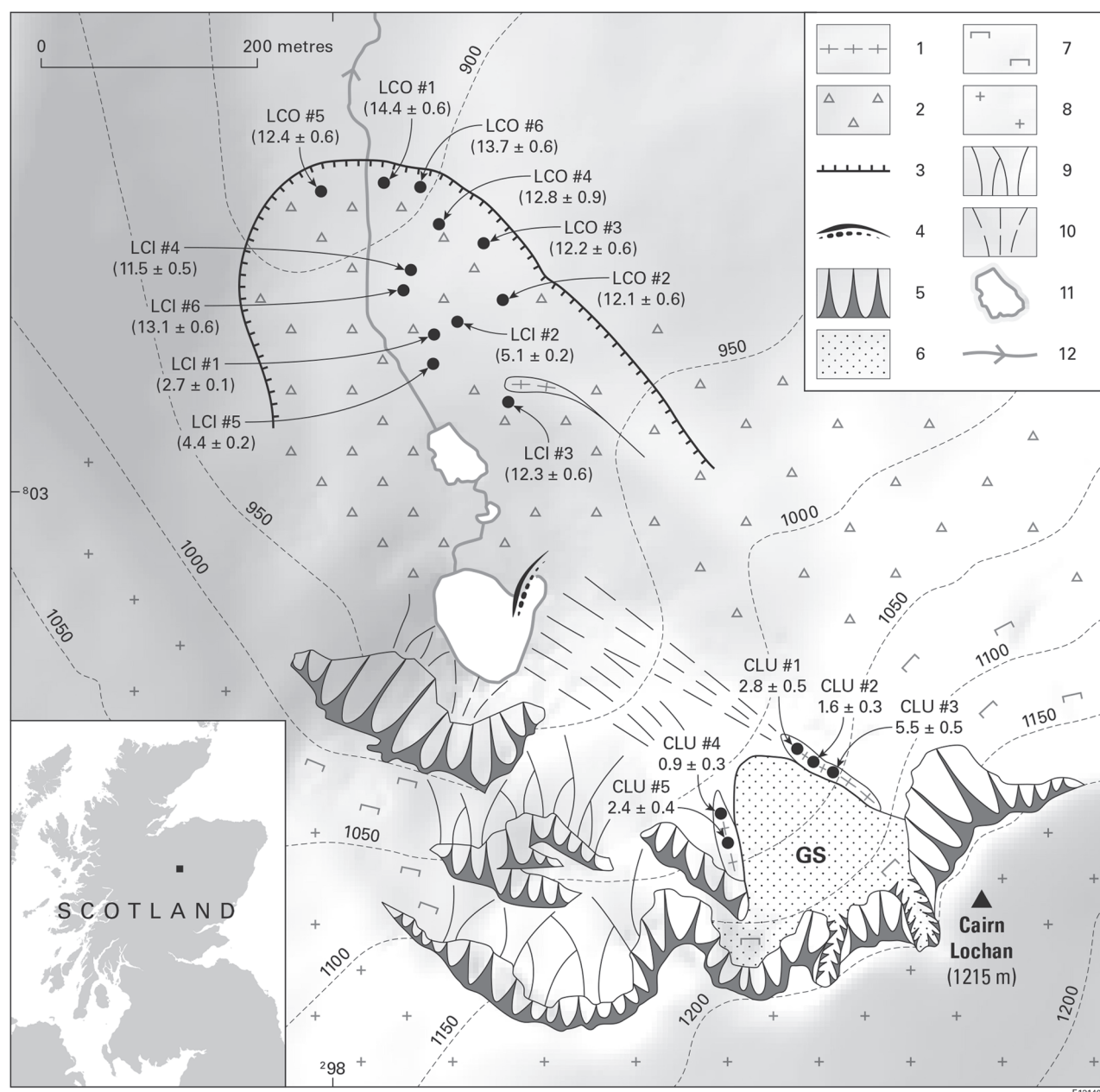Email: m.p.kirkbride@dundee.ac.uk

**Figure 1.** Geomorphology of Coire an Lochain showing the locations, sample numbers and exposure ages of ¹⁰Be samples and the former glacier extents in the cirque. Key: GS = Great Slab; 1 = moraine ridge crest; 2 = boulder sheet; 3 = margin of YDS till sheet; 4 = avalanche-impact pit; 5 = rock faces; 6 = rock slab; 7 = rock outcrops; 8 = frost-shattered mountain-top debris; 9 = scree slopes; 10 = polygenetic debris cones and avalanche aprons; 11 = lake and 12 = permanent stream. Contour lines are in metres above sea level. Easting and northing reference points refer to UK National Grid.

Slab, but form an opposing pair, and are interpreted as ice-marginal moraines.

The Great Slab (Figure 3b) is a source of full-depth snow avalanches in heavy-snow years, which are continuing to trim the lower ends and proximal slopes of the moraine ridges to deposit elongated splays of avalanche-reworked debris downslope (Figure 1). The avalanche debris apron extends to the lake (Figure 2), whose small eastern bay is interpreted as an avalanche-impact pit. Snow avalanches from the south-western cirque headwall onto lake ice have been observed to generate floods downstream through the till sheet (Bullivant, personal communication, 2011).

A glacial origin of the ridges is interpreted on the basis of their form and location. They contain matrix-supported angular granite clasts, up to boulder size, in a matrix of coarse sand and grit (Figure 3c). Boulder surfaces are pink in colour and markedly less edge-rounded compared with the grey weathered boulders on nearby slopes and till sheets (Figure 3a). Moraine boulders are smaller than

in the cirque-floor till sheets, and soil cover is thin with no horizon development. The ridges are oriented at a highly oblique angle to the headwall above, do not extend up to it and extend too far downslope for gravitational transport of debris across a firn field to have been the main debris source (cf. Ballantyne and Benn, 1994). For these reasons, a protalus origin for the ridges is discounted. No clast shape analysis has been conducted because a significant contribution to construction of the ridges may have come from reworking of pre-existing debris, which could have incorporated material with different transport histories. Thus, clast shape data are unlikely to provide diagnostic evidence of genesis.

## Field and laboratory methods

The location and relatively unweathered clasts of the Great Slab moraine indicates a significantly younger age than the cirque-floor till. Exposure-age dating was used (1) to test the presumed YDS

age for the latter, which was initially sampled with a view to investigating whether the whole deposit was of a single age, and (2) to investigate whether the Great Slab moraine represents evidence of a small Holocene glacier in the upper cirque. Rock samples were collected from large embedded boulders protruding from the moraine (Figure 3c), to avoid more recent debris deposited on the ridge surface by rockfall or snow avalanches. Samples CLU#1 to CLU#3 were from the longer right-lateral moraine, and CLU#4 and CLU#5 from the left-lateral moraine. Six samples were collected from each of the inner and outer parts of the cirque-floor boulder till, labelled LCI#1 to LCI#6 and LCO#1 to LCO#6, respectively. All were from the upper surfaces of boulders large enough to protrude above the surrounding boulder layer to minimise snow shielding. Sample locations are shown in Figure 1.

Samples were processed at the Cosmogenic Isotope Analysis Facility (CIAF) in the Scottish Universities Environmental Research Centre (SUERC). Rock samples were crushed and ground, and quartz was separated from other minerals by mechanical (magnetic) and chemical (hexafluorosilicic acid treatment and hydrofluoric acid leaching) procedures. $^{10}$Be extraction and target preparation followed procedures modified from Kohl and



**Figure 2.** View from the north into Coire an Lochain. Moraine crests in the upper cirque are indicated by white dotted lines. Below the Great Slab, an apron of snow-avalanche and debris-flow debris extends downslope to the main cirque lake (just visible to the right). The bouldery till sheet of YDS is indicated.
GS: Great Slab.

Nishiizumi (1992) and Child et al. (2000). The $^{10}$Be/$^9$Be ratios were measured using the 5 MV accelerator mass spectrometer (AMS) at SUERC (Xu et al., 2010). The Be ratios were converted to nuclide concentration in quartz. Details of sample locations and analytical data are given in Table 1. We provide two sets of exposure ages (Table 2), both calculated using the Cronus-Earth online calculator v. 2.2 (http://hess.ess.washington.edu/). However, the first set is calculated using a global production rate (4.39 ± 0.37 atoms/g/yr; $L_m$ scaling) obtained from age-constrained calibration measurements (Balco et al., 2008). The use of these widespread calibrations points leads to an increase of the scaling uncertainties.

New local calibration sites indicate that the global production rate used in the Cronus-Earth calculator is too high (e.g. Balco et al., 2009; Fenton et al., 2011). The second set of exposure ages was calibrated using a locally derived $^{10}$Be production rate (NWH LPR12.2; Ballantyne and Stone, 2012; Fabel et al., 2012), which is lower than the global production rate and has lower uncertainties related to scaling (sea-level high-latitude production rate 3.99 ± 0.13 atoms g/yr; $L_m$ scaling). Thus, the $^{10}$Be ages calculated using the LPR (Table 2) are older and more precise than $^{10}$Be ages calculated with the global production rate. Although the NWH LPR12.2 is not independently constrained, it corresponds closely to the Loch Lomond production rate (LLPR) of 3.92 ± 0.18 atoms/g/yr ($L_m$ scaling; Fabel et al., 2012). The LLPR is based on the $^{10}$Be concentration from boulders on the Loch Lomond terminal moraine and is independently constrained by radiocarbon dating (MacLeod et al., 2011).

## Results

### Chronology

The whole cirque-floor till sheet yields ages consistent with deposition in the YDS (Table 2). For the inner area of till (samples LCI#1 to LCI#6), the LPR calibration gives three ages of between 11.5 ± 0.5 and 13.1 ± 0.6 kyr (mean = 12.3 kyr). Three samples yield mid-Holocene ages of between 2.7 and 5.1 kyr. These boulders are interpreted to have been overturned after deposition either by snow avalanching from the western slopes of the cirque, or by avalanche-generated flood waves from the lake (freshly avalanche-disturbed boulders were observed nearby after the 2009–2010 winter). Four of the six samples from the outer till range in age from 12.1 to 12.8 kyr; the other two (LCO#1: 14.4 kyr and LCO#6: 13.7 kyr) may be inherited ages from older foreland debris incorporated into the YDS till close to the maximum of the advance. The mean age of samples LCI3, LCI4, LCI6, and LCO2 to LCO5 is 12.3 kyr – several centuries older than the dated
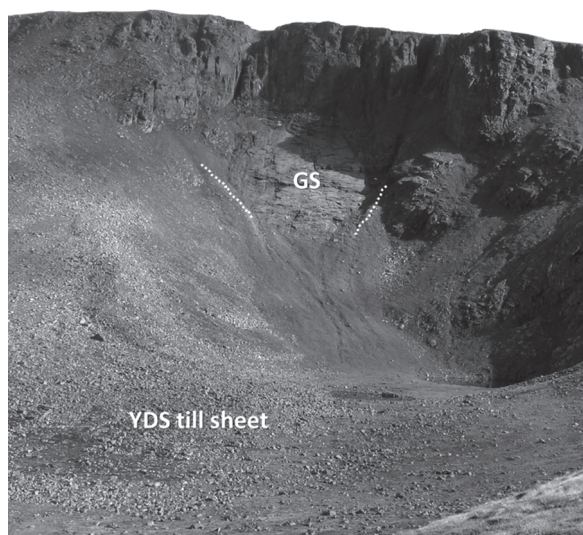


**Figure 3.** Details of the late-Holocene glacial landforms in the upper part of Coire an Lochain. (a) Looking south-west to the prominent right-lateral moraine on the near side of the Great Slab. Note the absence of debris accumulation between the slab and the headwall in (b) view from the left to the right-lateral moraine, across the plucked steps of the Great Slab. The right-lateral moraine is the steep grassy boulder ridge at the far side of the slab – (c) a boulder, embedded in the late-Holocene right-lateral moraine, sampled for $^{10}$Be dating.

**Table 1.** Sample locations and analytical details for the late-Holocene moraine (CLU) and the YDS till sheet (LCI and LCO).

| Sample | AMS ID | Latitude (°N) | Longitude (°W) | Altitude (m) | Thickness (cm) | Density (g/cm) | Shielding (factor)[a] | $^{10}$Be ± σ (atoms/g quartz)[b] |
|---|---|---|---|---|---|---|---|---|
| CLU#01 | b6524 | 57.1043 | −3.678 | 1040 | 2 (0.9833) | 2.7 | 0.9205 | 27,772 ± 3353 |
| CLU#02 | b6525 | 57.1044 | −3.678 | 1052 | 3 (0.9751) | 2.7 | 0.9205 | 16,513 ± 1723 |
| CLU#03 | b6526 | 57.1044 | −3.678 | 1043 | 4 (0.967) | 2.7 | 0.9205 | 54,292 ± 3858 |
| CLU#04 | b6527 | 57.1036 | −3.6796 | 1043 | 5 (0.959) | 2.7 | 0.8646 | 7945 ± 1273 |
| CLU#05 | b6531 | 57.1037 | −3.6794 | 1036 | 4 (0.967) | 2.7 | 0.8646 | 22,140 ± 2491 |
| LCI#1 | b2447 | 57.1 | −3.68 | 896 | 5 (0.959) | 2.7 | 0.9888 | 27,628 ± 1139 |
| LCI#2 | b2448 | 57.1 | −3.68 | 922 | 1 (0.9916) | 2.7 | 0.9853 | 54,096 ± 1588 |
| LCI#3 | b2353 | 57.1 | −3.68 | 914 | 1 (0.9916) | 2.7 | 0.9867 | 129,395 ± 3869 |
| LCI#4 | b2354 | 57.1 | −3.68 | 903 | 1 (0.9916) | 2.7 | 0.9854 | 120,034 ± 3299 |
| LCI#5 | b2355 | 57.1 | −3.68 | 896 | 1 (0.9916) | 2.7 | 0.9826 | 46,081 ± 1720 |
| LCI#6 | b2356 | 57.1 | −3.68 | 899 | 1 (0.9916) | 2.7 | 0.987 | 135,747 ± 4359 |
| LCO#1 | b2359 | 57.1 | −3.68 | 915 | 2.5 (0.9792) | 2.7 | 0.9824 | 149,051 ± 3450 |
| LCO#2 | b2349 | 57.1 | −3.68 | 917 | 2 (0.9833) | 2.7 | 0.9824 | 125,882 ± 3803 |
| LCO#3 | b2360 | 57.1 | −3.68 | 924 | 2 (0.9833) | 2.7 | 0.9798 | 127,762 ± 3805 |
| LCO#4 | b2350 | 57.1 | −3.68 | 916 | 5 (0.959) | 2.7 | 0.98 | 129,841 ± 7664 |
| LCO#5 | b2361 | 57.1 | −3.68 | 915 | 3 (0.9751) | 2.7 | 0.9824 | 127,517 ± 3837 |
| LCO#6 | b2362 | 57.1 | −3.68 | 909 | 2 (0.9833) | 2.7 | 0.985 | 141,717 ± 4074 |

[a]Shielding by distant objects after Dunne et al. (1999).
[b]$^{10}$Be/$^{9}$Be blank-corrected ratios and $^{10}$Be concentrations are referenced to NIST SRM 4325 (2.79 × 10$^{11}$; Nishiizumi et al., 2007). The processed blank $^{10}$Be/Be ratios were generally between 2% and 18% (two ratios of 25% and 41%) of the sample $^{10}$Be/Be ratios and were subtracted from the measured ratios. Uncertainties (±1σ) include all known sources of analytical error.

**Table 2.** Exposure ages and associated analytical uncertainties based on global and local production rates.

| Sample | Global PR | | | NWH 12.2 LPR | | |
|---|---|---|---|---|---|---|
| | Exposure age (kyr) | Internal σ (kyr) | External σ (kyr) | Exposure age (kyr) | Internal σ (kyr) | External σ (kyr) |
| CLU#1 | 2475 | 403 | 457 | 2779 | 452 | 462 |
| CLU#2 | 1467 | 264 | 293 | 1647 | 296 | 302 |
| CLU#3 | 4919 | 430 | 608 | 5524 | 483 | 518 |
| CLU#4 | 768 | 267 | 275 | 862 | 299 | 301 |
| CLU#5 | 2139 | 339 | 386 | 2400 | 380 | 389 |
| LCI#1 | 2425 | 100 | 234 | 2722 | 113 | 145 |
| LCI#2 | 4519 | 133 | 416 | 5076 | 150 | 228 |
| LCI#3 | 10944 | 331 | 1017 | 12301 | 373 | 562 |
| LCI#4 | 10253 | 285 | 945 | 11523 | 321 | 507 |
| LCI#5 | 3944 | 148 | 374 | 4429 | 166 | 224 |
| LCI#6 | 11633 | 378 | 1091 | 13077 | 426 | 617 |
| LCO#1 | 12833 | 301 | 1170 | 14428 | 339 | 599 |
| LCO#2 | 10752 | 329 | 1000 | 12084 | 370 | 554 |
| LCO#3 | 10877 | 328 | 1011 | 12226 | 369 | 557 |
| LCO#4 | 11411 | 682 | 1213 | 12826 | 768 | 884 |
| LCO#5 | 11003 | 335 | 1024 | 12367 | 377 | 566 |
| LCO#6 | 12173 | 355 | 1129 | 13685 | 399 | 615 |

PR: production rate.
Sample thickness correction using a rock density of 2.7 g/cm and attenuation length of 160 g/cm.
Exposure ages calculated using the $L_m$ scaling schemes in the Cronus-Earth (http://hess.ess.washington.edu/). Global PR ages was assumed to be 4.39 ± 0.37 atoms/g/yr. NWH LPR12.2 exposure ages are calculated using a production rate of 3.99 ± 0.13 atoms/g/yr based on a deglaciation age of 12.2 kyr in Scotland (Ballantyne and Stone, 2012; Fabel et al., 2012).
The calculated age uncertainties are expressed as 1σ. The external uncertainties include the internal (analytical) and the total (including calibration and scaling) uncertainties.

YDS maximum at the type site in the south-western Scottish Highlands (MacLeod et al., 2011).

Five $^{10}$Be ages from the Great Slab moraine (Table 2) range from 0.9 ± 0.3 years (CLU#4) to 5.5 ± 0.5 years (CLU#3) using the LPR calibration: four are younger than 2.8 ± 0.5 kyr. The wide spread of ages is interpreted as an effect of isotopic inheritance. Low rockfall rates in the Holocene (Ballantyne and Harris, 1994) would logically be associated with variable concentrations of

cosmogenic beryllium in cliff faces, whose exposed surfaces will comprise a mosaic of small facets of very different exposure ages. Rock falls can therefore be expected to contain varying concentrations of cosmogenic beryllium which are inherited by the moraine ridges following a short glacial transport path. It follows that $^{10}$Be ages should be interpreted as maximum ages for the moraines, and that the youngest boulder sampled provides the closest chronological control on moraine age. By this reasoning,
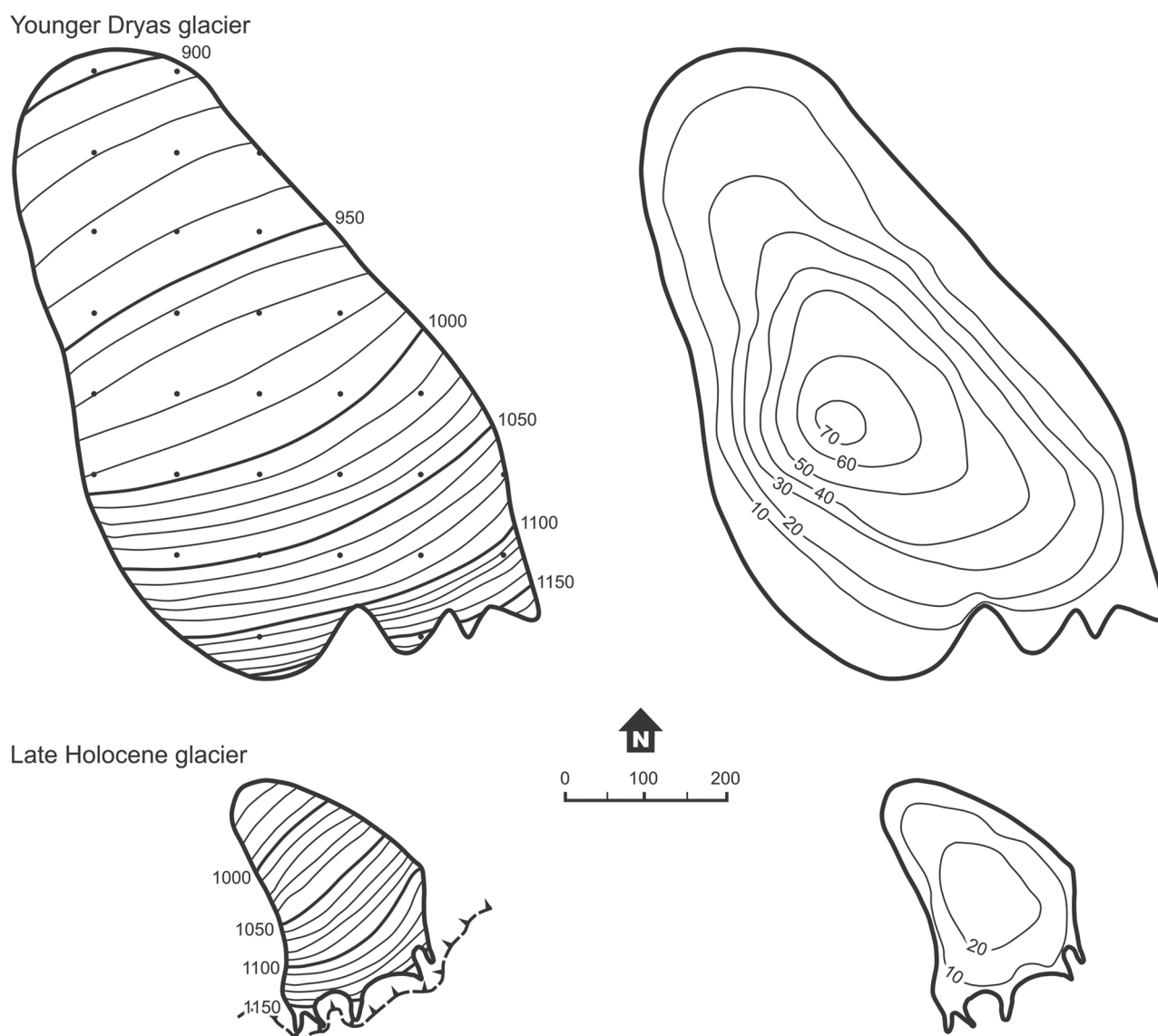
**Figure 4.** Reconstructions of the Younger Dryas (top) and late-Holocene (bottom) glaciers in Coire an Lochain, to the same scale. Surface topography is shown on the left, and ice thickness on the right, each with a 10 m contour interval.

the maximum moraine age lies between *c*. AD 850 and AD 1450 based on CLU#4 and deposition during the LIA is possible. A more cautious approach is to regard CLU#3 as an outlier, in which case, the earliest possible age for the moraine is <2.8 kyr, during or after the climatic deterioration of the Sub-Atlantic period, but as discussed below, this does not discount an LIA age for the glacier.

*Glacier reconstruction and climatic implications*

Glacier morphology was reconstructed at a scale of 1:6250 and contoured at a 10 m interval, from which surface slopes and hypsometric curves were calculated and former equilibrium lines estimated using an accumulation area ratio of 0.6 (Figure 4). Isopach maps were constructed by subtraction of present-day relief from the former glacier surface topography by grid sampling of the reconstructed glacier surfaces. Glaciological reconstructions followed the method of Carr et al. (2010), based on the best-fit regressions of empirical relations from contemporary glaciers. An independent estimate of summer (June–August) temperature was used to calculate total accumulation and winter balance at the equilibrium line altitude (ELA) of each glacier. Accumulation is used to estimate ablation gradients, which are in turn applied to the hypsometric curves to estimate mass loss per

altitudinal band of each ablation zone (mean annual ablation multiplied by the area between contour lines). In equilibrium mass balance, total mass loss from an ablation zone equates to the balance discharge through the ELA, which divided by cross-sectional area gives the balance velocity. The creep velocity equation of Paterson (1994) is then applied to calculate the average rate of ice flow due to deformation, using flow law parameters of $n = 3$ (exponent) and $5.3 \times 10^{-15}/s/kPa^n$ (constant). The latter value is for temperate ice so a lower value may be appropriate for the YDS glacier, in which case the present results will overestimate creep velocity. Average sliding velocities through the ELA are estimated as the difference between the balance and creep velocities.

The mean summer ELA temperature for the late-Holocene glacier was taken as the present (1981–2000) temperature minus 1.5°C (see Harrison et al., forthcoming). Present-day temperature was based on Aviemore weather data recorded at 228 m altitude, adjusted to the ELA using an empirical lapse rate of 0.007°C/m calculated from the temperature difference between Aviemore and Cairngorm summit (1245 m, 2.5 km to the east-northeast). The mean summer temperature for the YDS glacier ELA was derived from a contemporary chironimid-based mean July temperature of 6.8°C (from Brooks et al., 2012) from Abernethy Forest, 230 m a.s.l. and 15 km to the north. The mean July temperature was

**Table 3.** Reconstructed climatic and glaciological parameters for the Coire an Lochain glaciers, following the method of Carr et al. (2010).

| Variable | Late-Holocene glacier | YDS glacier | Units |
|---|---|---|---|
| Glacier area | 36,200 | 310,500 | m² |
| Glacier volume | 456,000 | 9,625,000 | m³ |
| ELA | 1047 | 963 | m |
| Mean July ELA temperature | 6.9 | 1.7 | °C |
| Mean June–August ELA temperature | 6.0 | 0.8 | °C |
| Mean May–October ELA temperature | 4.1 | −1.1 | °C |
| Winter balance at ELA | 2.3 | 0.6 | m/yr |
| Total accumulation at ELA | 2.7 | 0.9 | m/yr |
| Ablation gradient | −0.0076 | −0.0034 | m/m/yr |
| Balance velocity | 1.4 | 0.7 | m/yr |
| %Basal sliding | 85 | 58 | % |
| Average τ | 61 | 58 | kPa |

YDS: Younger Dryas Stadial; ELA: equilibrium line altitude.

adjusted to a June–August average using their present-day ratio, and then to the ELA using the same lapse rate. The YDS July temperature at 230 m altitude was 7.3°C cooler than the present day.

The results of the glaciological and climatic reconstructions are shown in Table 3. The startling statistic is the three-fold decrease in precipitation and accumulation values in the YDS, associated with ablation-season temperatures close to freezing and very low turnover. In contrast, the late-Holocene glacier required high winter accumulation to sustain the glacier through summers averaging 4.1°C across the ablation season, and 6.9°C for July. Similar average shear stresses between the two glaciers mask the contrast between a thin, steep and more dynamic late-Holocene glacier in which 85% of motion was through basal sliding on a smooth, impermeable rock slab, and a thicker, colder and less dynamic YDS glacier, which existed in a cold continental environment (Table 3). One commonality between the glaciers is that both depended strongly on enhanced accumulation by blown snow from the surrounding plateau (Harrison et al., forthcoming; Sissons, 1979). This offset the aridity of the YDS and the warmth of the late Holocene to allow glaciers to form and survive in each period.

In Carr et al.'s (2010) method, sliding velocity is pragmatically a residual value after other parameters have been calculated, and is ultimately dependent on the best-fit summer temperature-accumulation regression. Ohmura et al.'s (1992) relation of June–August temperature and approximate annual precipitation (winter accumulation plus summer precipitation at ELA) includes the standard deviations around the best-fit curve, allowing a range of possible precipitation scenarios to be modelled. Taking the June–August ELA temperature of 6.0°C for the late-Holocene glacier (Table 3), Ohmura et al.'s relation also yields an annual precipitation value of $c$. 2.70 m/yr but with a ±1σ range of 2.25–3.25 m/yr. At the upper end of this range, mass turnover in the Coire an Lochain glacier could therefore have been 20% greater, with a higher sliding velocity to maintain equilibrium.

Reconstruction of the late-Holocene glacier gives results that are climatically and glaciologically credible. However, the question remains as to whether a small accumulation zone of 27,500 m² combined with a high accumulation rate was able to hold firn for a sufficiently long period to form glacier ice above the ELA. This question is addressed by comparing an estimated mean residence time of snow and ice in the accumulation zone with the time taken for attainment of the firn–ice transition (a density of 0.85 g/cm³: Paterson, 1994). For a calculated accumulation-zone

volume of 413,000 m³ and a balance discharge through the ELA of 4150 m³/yr, the mean residence time would have been $c$. 100 years. In temperate glacial environments where saturation of the snowpack occurs, the firn–ice transition can be reached in as little as 5–7 years (Paterson, 1994). Glacier ice therefore would have formed quickly above the ELA.

However, a residence time of $c$. 100 years also requires the glacier to have survived for longer than this in order to construct moraines at lower altitude, and this may pose a problem given the marginal conditions for glaciation in the late Holocene. The possibility exists that the glacier may not be accurately represented by Carr et al.'s model due to its thin, steep form and smooth impermeable bed: conditions of high shear stress combined with low normal stress promote effective basal pressure variations and bed separation (Benn and Evans, 2010). A significantly higher mass turnover may have been possible if sliding velocity was faster, sustained by greater local wind-blown enhancement of accumulation than the above calculations have estimated. By back-calculating from balance velocity to the mean specific net accumulation required to maintain equilibrium, a balance velocity of 5 m/yr would require net accumulation of only 0.67 m/yr with a 27 years accumulation-zone residence time. Corresponding values for a balance velocity of 10 m/yr are 1.34 m/yr and 14 years. These scenarios seem more plausible, and would have allowed the glacier to construct moraines within a lifespan of much less than 100 years, although ablation would also have to be greater than calculated by the Carr et al. method.

## Discussion: A LIA glaciation in the Cairngorm Mountains?

The orbitally driven decline in Holocene temperatures since the Climatic Optimum (Mayewski et al., 2004; Wanner et al., 2008, 2011) led to the earliest neoglacial glacier advances in high-latitude and high-altitude mountains in Europe and Scandinavia, where the terrain was high enough for the glaciation threshold to be crossed at earlier stages of the mid-Holocene cooling. Subsequent cooling led to a later onset of neoglacial advances in lower ranges. The Scottish Highlands were only approaching the glaciation threshold late in the Holocene. Our results demonstrate that a small glacier existed in the upper cirque of Coire an Lochain since $c$. 2.8 kyr, after snow-avalanche disturbance of YDS boulders since the mid-Holocene. This finding is the first firm evidence of Holocene glacier formation in the British Isles. The glacioclimatic reconstruction shows that the ELA lay closer, in altitudinal terms, to the YDS glacier than a simple temperature driver would allow. This emphasises both the importance of enhanced precipitation for allowing glacier ice to form (Harrison et al., forthcoming), and the aridity of YDS winters in the Cairngorm Mountains.

A question of great interest is whether the glacier existed during the period of LIA glacierisation (sensu Matthews and Briffa, 2005) after AD 1300. Local low and high-altitude proxy temperature records (Barber et al., 1999; Dalton et al., 2005) show a general cooling throughout the second half of the Holocene, so that glacier formation prior to 2.8 kyr (if samples CLU#1 to CLU#5 are accepted as maximum ages) is highly unlikely. However, these records have insufficient chronological control to judge when the greatest sustained cooling occurred within the last 2.8 millennia. While there is a general view that the post-Mediaeval cooling exceeded earlier cool periods (Wanner et al., 2011), palaeoecological records from the Netherlands (Van Geel et al., 1996) and Switzerland (Hieri et al., 2003; Larocque-Tobler et al., 2010) indicate cooler temperatures in the Sub-Atlantic period than during the last 500 years. Thus, the Holocene proxy temperature record does not appear to provide a clear cold 'spike' with which to correlate the late-Holocene glacier. From historical climatology, the

decade AD 1690–1700 is generally regarded as having had the lowest air temperatures throughout the period AD 1350–1700 across northern Europe (Lamb, 1995). The period was associated with a marked decrease in sea-ice cover across the northern North Atlantic and Greenland Sea that had the effect of displacing the polar oceanic and atmospheric fronts to the south (Lamb, 1995). There is also limited evidence that the exceptional cold and increased winter snowfall that characterised this period was associated with a predominance of easterly and northeasterly winds during winter (Dawson, 2009). Similar, although less extreme conditions, prevailed across Scotland for much of the 18th century, culminating in the extreme cold of the 1780s.

A significant question is whether the long, snowy winters of the late 17th and 18th centuries occurred frequently enough to generate and sustain glacier ice for a sufficient period to form moraine ridges. Several summaries of historical climate (Dawson, 2009; Kington, 2010; Lamb, 1995) concur that the late 17th and 18th centuries experienced the most sustained 'glacier-friendly' climates, and several periods when climate approached glaciation are noted by Lamb (1995) and Kington (2010). The central England temperature series (Lamb, 1995) places the greatest post-Mediaeval cool temperatures within this period. We suggest here that the period AD 1650–1790 was the most conducive time for glacier formation in Scotland during the last *c*. 2.8 kyr, when the North Atlantic Oscillation was dominantly in negative mode (Luterbacher et al., 2002). The glacier described here probably constructed its moraines within this interval, and may have survived until the mid-19th century. Peat-based proxies of wetness from northern Britain, including sites in the Cairngorm Mountains, indicate high water tables and greater humidity around AD 1640, between AD 1715 and 1850, and between AD 1790 and 1830 (Barber et al., 1999; Blundell and Barber, 2005; Mauquoy et al., 2008). These periods would have been associated with greater snow accumulation on the Cairngorm Plateau.

The glaciological reconstruction of the late-Holocene glacier creates a picture of a thin, steep, sliding glacier existing close to the limit of climatic viability, facilitated by enhanced snow accumulation, rapid transformation to glacier ice, and short ice residence time. Thus, construction of small ice-marginal moraines would have been aided by a rapid supply of debris to the ablation zone margin. The location of the Holocene glacier is unusual to the extent that we suspect there would have been very few, if any, similar topoclimatic niches in the British mountains where contemporary late-Holocene glaciers could have formed (cf. Harrison et al., forthcoming). The glacier existed partly because the Great Slab supported an accumulation zone on a relatively low-angle surface above 1050 m altitude. The upper cirque is narrowly enclosed by vertical faces, providing effective shading for such a small glacier, and accumulation enhancement by the extensive plateau above is very effective, even today. Only such a combination of geomorphological factors could allow marginal glaciation in recent millennia of a warm Atlantic Ocean and dominantly westerly cyclonic airflow. Conversely, altitudes of the main cirque floors in the Cairngorm Mountains appear to have been just too low to allow ice to survive for long enough to construct moraine ridges, and reconnaissance of several cirques has produced evidence of pronival deposition rather than Holocene moraines.

In conclusion, this study has demonstrated the former presence of a glacier ice in the British Isles in the late Holocene. It seems probable that a glacier existed in Coire an Lochain in the LIA. However, few other sites in the Cairngorm Mountains are likely to have correlative moraines due to stringent topoclimatic criteria that would have been needed to be met. Glacioclimatic reconstructions highlight the extremes of glaciological environment represented by the Younger Dryas cirque glacier and the late-Holocene niche glacier. The irony is that the elusive landform

evidence for recent glacial activity was discovered in one of the most visible locations in the massif.

## References

Balco B, Stone J, Lifton N et al. (2008) A simple, internally consistent, and easily accessible means of calculating surface exposure ages and erosion rates from Be-10 and Al-26 measurements. *Quaternary Geochronology* 3: 174–195.

Balco G, Briner J, Finkel RC et al. (2009) Regional beryllium-10 production rate calibration for late-glacial northeastern North America. *Quaternary Geochronology* 4: 93–107.

Ballantyne CK (2013) Lateglacial rock-slope failures in the Scottish Highlands. *Scottish Geographical Journal* 129: 67–84.

Ballantyne CK and Benn DI (1994) Glaciological constraints on protalus rampart development. *Permafrost and Periglacial Processes* 5: 145–153.

Ballantyne CK and Harris C (1994) *The Periglaciation of Great Britain*. Cambridge: Cambridge University Press, 303 pp.

Ballantyne CK and Stone JO (2012) Did large ice caps persist on low ground in north-west Scotland during the Lateglacial Interstade? *Journal of Quaternary Science* 27: 297–306.

Barber KE, Batterbee RW, Brooks SJ et al. (1999) Proxy records of climate change in the UK over the last two millennia: Documents change and sedimentary records from lakes and bogs. *Journal of the Geological Society of London* 156: 369–380.

Batterbee RW, Cameron NG, Golding P et al. (2001) Evidence for Holocene climatic variability from sediments of a Scottish remote mountain lake. *Journal of Quaternary Science* 16: 339–346.

Benn DI and Evans DJA (2010) *Glaciers and Glaciation*. 2nd Edition. London: Hodder Arnold, 802 pp.

Blundell A and Barber K (2005) A 2800-year palaeoclimatic record from Tore Hill Moss, Strathspey, Scotland: The need for a multi-proxy approach to peat-based climate reconstructions. *Quaternary Science Reviews* 24: 1261–1277.

Brooks SJ, Matthews IP, Birks HH et al. (2012) High-resolution Lateglacial and early Holocene summer air temperature records from Scotland inferred from chironomid assemblages. *Quaternary Science Reviews* 41: 67–82.

Carr SJ, Lukas S and Mills SC (2010) Glacier reconstruction and mass-balance modelling as a geomorphic and palaeoclimatic tool. *Earth Surface Processes and Landforms* 35: 1103–1115.

Child D, Elliott G, Mifsud C et al. (2000) Sample processing for earth science studies at ANTARES. *Nuclear Instruments & Methods in Physics Research Section B: Beam Interactions with Materials and Atoms* 172: 856–860.

Dalton C, Birks HJB, Brooks SJ et al. (2005) A multi-proxy study of lake-development in response to catchment changes during the Holocene at Lochnagar, north-east Scotland. *Palaeogeography, Palaeoclimatology, Palaeoecology* 221: 175–201.

Dawson A (2009) *So Foul and Fair a Day: A History of Scotland's Weather and Climate*. Edinburgh: Birlinn, 230 pp.

Dunne A, Elmore D and Muzikar P (1999) Scaling of cosmogenic nuclide production rates for geometric shielding at depth on sloped surfaces. *Geomorphology* 27: 3–11.

Fabel D, Ballantyne C and Xu S (2012) Trimlines, blockfields, mountain-top erratics and the vertical dimensions of the last British-Irish Ice Sheet in NW Scotland. *Quaternary Science Reviews* 55: 91–102.

Fenton CR, Hermanns RL, Blikra LH et al. (2011) Regional $^{10}$Be production rate calibration for the past 12 ka deduced from the radiocarbon-dated Grøtlandsura and Russenes rock avalanches at 69° N, Norway. *Quaternary Geochronology* 6: 437–452.

Golledge NR, Hubbard A and Sugden DE (2008) High-resolution numerical simulation of the Younger Dryas glaciation in Scotland. *Quaternary Science Reviews* 27: 888–904.

Harrison S, Rowan AV, Glasser NF et al. (forthcoming) Little Ice Age glaciers in Britain: Glacier-climate modelling in the Cairngorm Mountains. *The Holocene*. DOI: 10.1177/0959683613516170.

Hieri O, Lotter AF, Hausmann S et al. (2003) A chironomid-based Holocene summer air temperature reconstruction from the Swiss Alps. *The Holocene* 13: 477–484.

Kington J (2010) *Climate and Weather*. London: HarperCollins, 484 pp.

Kohl C and Nishiizumi K (1992) Chemical isolation of quartz for measurement of in situ-produced cosmogenic nuclides. *Geochimica et Cosmochimica Acta* 56: 3586–3587.

Lamb HH (1995) *Climate History and the Modern World*. London and New York: Routledge, 433 pp.

Larocque-Tobler I, Heiri O and Wehrli M (2010) Late Glacial and Holocene temperature changes at Egelsee, Switzerland, reconstructed using subfossil chironomids. *Journal of Paleolimnology* 43: 649–666.

Luterbacher J, Xoplaki E, Dietrich D et al. (2002) Extending North Atlantic Oscillation reconstructions back to 1500. *Atmospheric Research Letters* 2: CXXIX–CXXXIX.

MacLeod A, Palmer A, Lowe J et al. (2011) Timing of glacier response to Younger Dryas climatic cooling in Scotland. *Global and Planetary Change* 79: 264–274.

Manley G (1949) The snowline in Britain. *Geografiska Annaler* 31: 179–193.

Matthews JA and Briffa K (2005) The 'Little Ice Age': Re-evaluation of an evolving concept. *Geografiska Annaler Series A: Physical Geography* 87: 17–36.

Mauquoy D, Yeloff D, van Geel B et al. (2008) Two decadally-resolved records from north west European peat bogs show rapid climate changes associated with solar variability during the mid-late Holocene. *Journal of Quaternary Science* 23: 745–763.

Mayewski PA, Rohling EE, Curt Stager J et al. (2004) Holocene climatic variability. *Quaternary Research* 62: 243–255.

Nishiizumi K, Imamura M, Caffee M et al. (2007) Absolute calibration of Be-10 AMS standards. *Nuclear Instruments & Methods in Physics Research Section B: Beam Interactions with Materials and Atoms* 258: 403–413.

Ohmura A, Kasser P and Funk M (1992) Climate at the equilibrium line of glaciers. *Journal of Glaciology* 38: 397–411.

Paterson WSB (1994) *The Physics of Glaciers*. Oxford: Pergamon Press, 480 pp.

Rapson SC (1985) Minimum age of corrie moraine ridges in the Cairngorm Mountains, Scotland. *Boreas* 14: 155–159.

Sissons JB (1979) The Loch Lomond Advance in the Cairngorm Mountains. *Scottish Geographical Magazine* 95: 66–93.

Sugden DE (1977) Did glaciers form in the Cairngorms in the 17th–19th centuries? *Cairngorm Club Journal* 18: 189–201.

Van Geel B, Buurman J and Waterbolk HT (1996) Archaeological and palaeoecological indications of an abrupt climate change in The Netherlands, and evidence for climatological teleconnections around 2650 BP. *Journal of Quaternary Science* 11: 451–460.

Wanner H, Beer J, Bütikofer J et al. (2008) Mid- to late Holocene climate change: An overview. *Quaternary Science Reviews* 27: 1791–1828.

Wanner H, Solomina O, Grosjean M et al. (2011) Structure and origin of Holocene cold events. *Quaternary Science Reviews* 30: 3109–3123.

Xu S, Dougans AB, Freeman SPHT et al. (2010) Improved Be-10 and Al-26 AMS with a 5 MV spectrometer. *Nuclear Instruments & Methods in Physics Research Section B: Beam Interactions with Materials and Atom* 268: 736–738.